

## Electronic Supporting Information

### Unravelling nanostructured Nb-doped TiO<sub>2</sub> dual band behaviour in smart windows by *in-situ* spectroscopies.

Miguel García-Tecedor<sup>a</sup>, Giulio Gorni<sup>b</sup>, Freddy Oropeza<sup>a</sup>, Laura Gómez<sup>a</sup>, Marta Liras<sup>a</sup>, Victor A. de la Peña O'Shea<sup>\*a</sup> and Mariam Barawi<sup>\*a</sup>

(a) Photoactivated Processes Unit, IMDEA Energy Institute. Avda. Ramón de la Sagra, 3. 28935 Móstoles (Madrid) Spain.

(b) CELLS-ALBA Synchrotron, carrer de la LLum, 2-26, 08290, Cerdanyola del Vallès (Barcelona) Spain.

**Keywords:** Colloidal nanocrystals, electrochromism, localized surface plasmon resonance, smart windows, electrochemical impedance spectroscopy, in situ spectroelectrochemistry, in situ XAS.

#### Table of Contents

S1. Materials .....	2
S2. Experimental methods .....	2
Synthesis procedure .....	2
Viscous paste formulation and thin film preparation .....	2
Smart windows device fabrication .....	2
Characterisation techniques .....	3
S3. Colloidal NCs characterisation .....	5
S4. Thin film preparation and characterisation .....	7
Thin film cross section .....	7
EDX analysis of the NCs thin films .....	8
S5. <i>Ex situ</i> XANES Ti Edge .....	9
S6. <i>Ex situ</i> XANES Nb-edge and DFT calculations .....	10
S7. Electrochemical properties of bare and Nb doped TiO <sub>2</sub> .....	11
S8. In situ XANES and NEXAFS .....	13
S9. In situ Nb Edge .....	15
S10. Electrochemical impedance Spectroscopy .....	15
S11. Smart window device .....	17

## S1. Materials

All the solvents and reagents used for the NCs synthesis were purchased by Merck: 1-Octadecene (ODE) 90%, 1-Octadecanol (95%), titanium ethoxide (TEO) technical grade, Niobium (V) ethoxide (99,5%), oleic acid (OAc) 68+% and hexane-(n) anhydrous (95+%).

Electrochemical electrolyte was composed by LiClO<sub>4</sub> battery grade, dry, 99.99% (Merck) trace metals basis and Propylene carbonate, anhydrous, 99.7% (Merck)

## S2. Experimental methods

### Synthesis procedure

The synthetic procedure was an adaptation of the procedure reported by de Trizio *et al.*<sup>1</sup> The reaction was carried out under argon atmosphere in Schleck line. In this sense, a mixture of octadecanol (ODAL) (3.52 g, 13 mmol), oleic acid (OAc) (0.32 mL, 1 mmol), and octadecene (ODE) (4 mL) was degassed under vacuum at 120 °C for 1 h in a Schleck (denominated Schleck 1). In a second Schleck (Schleck 2), we put 1mL of ODE and degassed it with argon during 10 minutes. After that, we add the titanium ethoxide (TEO) (0.19 mL, 0.9 mmol) and niobium ethoxide (0.025 mL, 0.1 mmol) and maintain it under stirring during 1 hour. Metal ethoxides are storage in inert atmosphere to avoid oxygen and humidity contamination. After the waiting time, content of Schleck 2 was injected on Schleck 1 with a transfer cannula while stirring and then raising the temperature to 290 °C during 60 min.

After that, the solution was cooling to room temperature, and the NCs were isolated from the reaction mixture by precipitation with acetone, separation of the solids and and redispersion in hexane, repeated several times. At each washing step, 100 µL of OAc were added to the NC hexane solution to prevent aggregation. Finally, the NCs were dispersed in 4 mL of hexane and add 25 µL of OAc to yield a stable colloidal solution. The obtained yield was 80% (~65 mg total NC were deduced by ICP while theoretical yield is 80 mg)

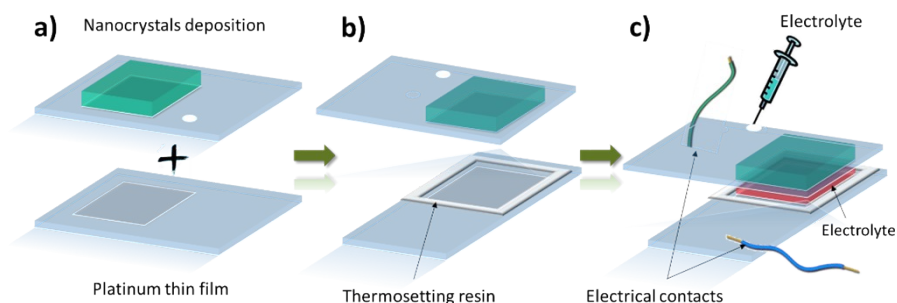
### Viscous paste formulation and thin film preparation

Pristine colloidal NCs suspended in hexane were turned into viscous pastes upon its addition on a solution of 10 wt. % of ethyl cellulose (30–70 mPa·s from Sigma-Aldrich) in  $\alpha$ -terpineol. The hexane was evaporated through a Rotavapor. The pastes were deposited by doctor blade on the ITO substrates and then calcinated at 430°C during 30 min in order to remove all organic compounds. The choice of ITO as transparent conductive oxide was the requirement to guarantee a high optical transmission over the full range of wavelengths. Upon thermal annealing at 430 °C the ITO-coated glass exhibited a high transmittance (averagely >82%) over both VIS and NIR regions, at the cost of a tolerable reduction of the electron conductivity (the resistance increased from ~20  $\Omega$ /sq to ~85  $\Omega$ /sq). Before NCs deposition, the substrates were cleaned via subsequent sonication steps: first in deionized water, then a mix of acetone and isopropyl alcohol.

### Smart windows device fabrication

NCs thin films was used as working electrodes in the home-made smart windows having a 1 cm<sup>2</sup> active area. The counter electrode was prepared by depositing a Pt thin platinum layer (<5 nm) by doctor blade (Dyesol PT1 viscous paste) on an ITO covered glass and subsequent thermal treatment at 430 °C. A thermoplastic gasket was used as sealant. The electrolyte was introduced

into the cell gap through a hole that had been predrilled on the back of the Pt-coated glass. The hole was finally sealed with a thermosetting resin.



**Scheme S1.** Lab scale smart windows device preparation.

### Characterisation techniques

**X-Ray Diffraction (XRD).** The crystal structure of bare and Nb doped TiO<sub>2</sub> was characterized by using a diffractometer Philips PW 3040/00 X'Pert MPD/MRD with Cu K<sub>α</sub> radiation ( $\lambda = 1.54178$  Å) at a scanning rate of 0.2° s<sup>-1</sup>. Samples for XRD were prepared on a Si substrate to avoid ITO and glass signal.

**Field Emission-Scanning Electron Microscopy (FE-SEM).** The morphology of the analyzed samples was studied with a Field Emission SEM JEOL JSM-7900F, using LED and BED-C detectors. For colloidal dispersion NCs the samples were drop on a specific grid and the images were acquired using STEM mode and operating at 30KV and a work distance (WD) of 9 mm. For the thin film samples, the images were acquired operating with 1 kV and a work distance (WD) between 2-10 mm. The EDX spectra were acquired with a ULTIM Max 170 from Oxford Instruments, equipped with Aztec software.

**Raman Spectroscopy** was performed with a Jasco NRS-5100 spectrometer using a laser of 532 nm of wavelength at 5.3 mW power.

**X-Ray Photoelectron Spectroscopy (XPS)** measurements were recorded on a lab-based spectrometer (SPECS GmbH, Berlin) using a monochromated AlK<sub>α</sub>1 source ( $h\nu = 1486.6$  eV) operating at 50 W. The X-rays are microfocused to give 300 μm a spot size on the samples. The spectrometer analyser is a SPECS PHOIBOS 150 NAP, a 180° hemispherical energy analyser with 150 mm mean radius. The entrance to the analyser is a nozzle with a 300 μm diameter orifice. The total energy resolution of the measurements was about 0.50 eV. The binding energy (BE) was calibrated against the Au Fermi level. Spectra were recorded in UHV as well as under H<sub>2</sub>O pressures of at 0.1 mbar, 0.5 mbar and 1 mbar.

**Ultraviolet–Visible Diffuse Reflectance Spectra (UV–Vis DRS)** for absorption of the colloidal NCs suspension were performed with a Perkin Elmer Lambda 1050 UV/Vis/NIR spectrometer.

### **X-ray Absorption Spectroscopy (XAS)**

X-ray absorption (XAS) spectra at Ti and Nb K-edge were measured at the CLAES beamline of the ALBA synchrotron [1] using a Si(111) and Si(311) double crystal monochromator, respectively. The harmonic rejection was achieved by a proper combination of angle and coating of collimating and focusing mirrors. The focus at the sample position was adjusted to be around

400 x 400  $\mu\text{m}^2$ . The beamline was calibrated with Ti and Nb foils measured in transmission mode and the incident and transmitted intensity measured using two ionization chambers filled to have approximately 10 and 75 % of absorption above the corresponding edges.

*Ex-situ* measurements of the samples were performed in total electron yield (TEY) using an aluminum sample holder and the sample glued to it by silver paint. The photocurrent was extracted with a metallic wire connected to the aluminum holder and the signal detected by an ionization chamber. Fluorescent measurements were recorded for comparison with a six channels silicon drift detector (Xpsress'3 from Quantum detector). *In-situ* experiments were performed using a home-made electrochemical cell with a volume of 20 ml with a kapton window. The spectra were recorded in fluorescence mode and the energy scans performed using an integration time of 0.1 s per point.

The data were analyzed by ATHENA and ARTEMIS software of the DEMETER package [3]. Simulation of the Nb K-edge X-ray absorption near edge-structure (XANES) spectrum was performed with the FDMNES software [4] using a cluster of 5.0 Å and the finite difference method (FDM) to solve the Schrödinger equation and avoid the muffin-tin approximation. The simulated spectrum was then convoluted to take into account the core-hole broadening and make the spectrum comparable with the measured one.

### **Computational details**

DFT calculations were carried out using the VASP5.4.4 code refs with projector-augmented wave (PAW) potentials refs to account for the core valence interaction. Niobium was substitutionally doped onto four Ti sites in a  $\text{TiO}_2$  supercell which consist of 3x3x2 unit cells for anatase ( $\text{Ti}_{72}\text{O}_{144}$ ). The total energies corresponding to the optimized geometries of all samples were calculated using the spin polarized version of the Perdew–Burke–Ernzerhof (PBE) refs The Heyd–Scuseria–Ernzerhof hybrid functional (HSE06) refs was used, with the exchange contribution set at 25% and the screening parameter set to 0.2 Å<sup>-1</sup>. No symmetry constraints were applied to the doped structures.

### **Electrochemical measures**

Electrochemical measures were performed in three electrode configuration, being bare and Nb doped  $\text{TiO}_2$  thin films the working electrodes and Pt and Ag wires the counter and reference electrodes respectively. A  $\text{Li}^+$  based electrolyte was used during all experiments (1M  $\text{LiClO}_4$  in propylene carbonate). An Ar flow was used to purge the system and maintain an inert atmosphere.

### S3. Colloidal NCs characterisation

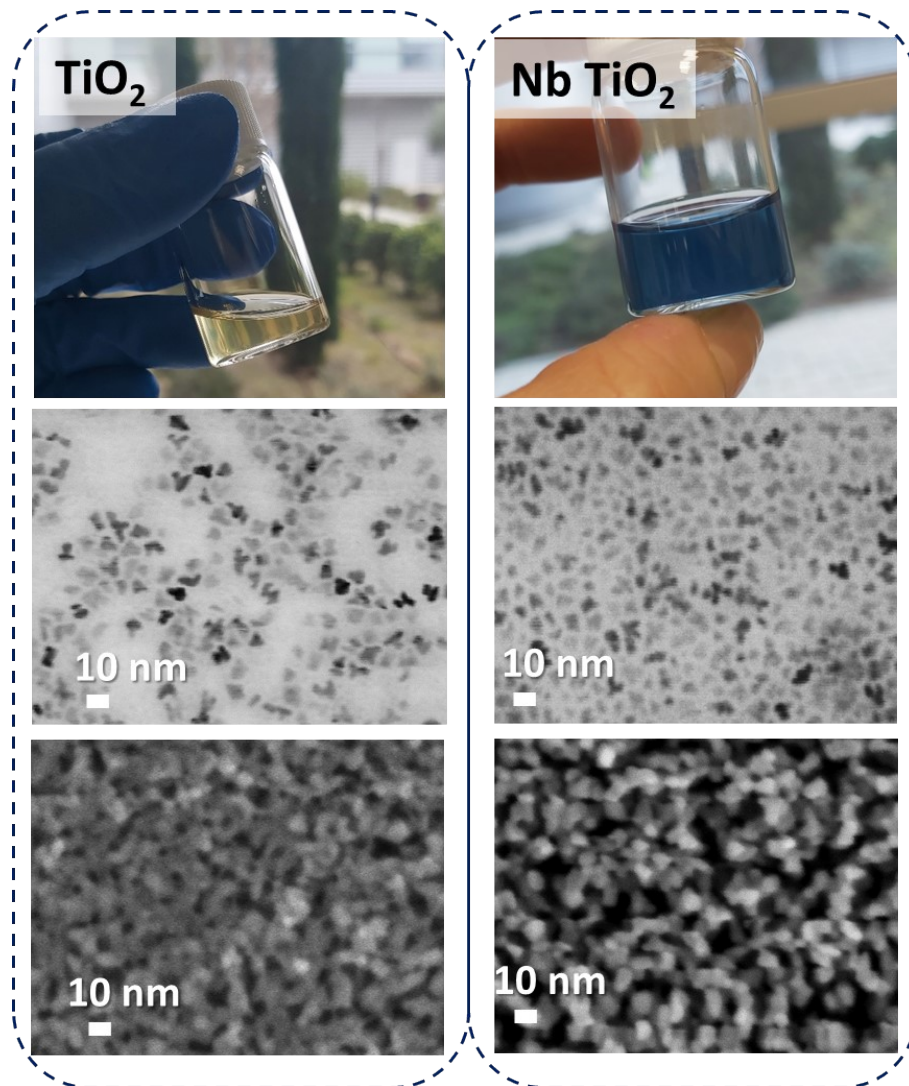


**Figure S1.** Comparative of Colloidal suspension and FESEM images in STEM mode and FESEM mode of bare and Nb doped  $\text{TiO}_2$  as colloidal suspension and thin film, respectively

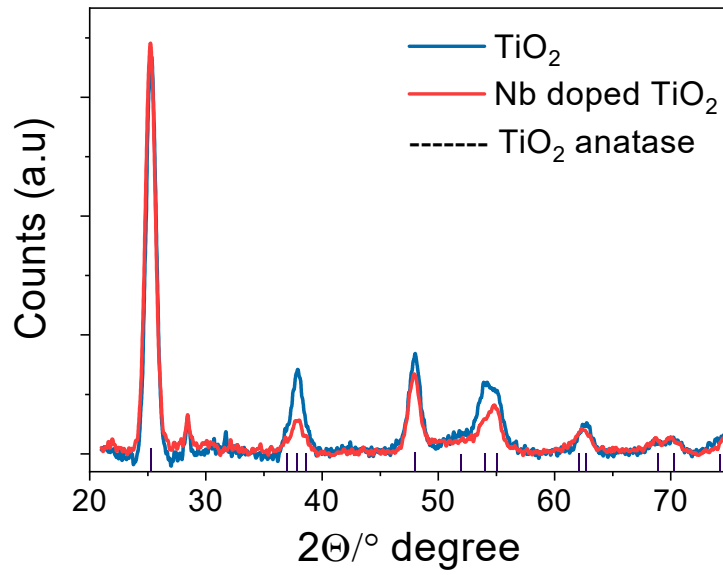


**Figure S2.** XRD diffractogram of bare (blue) and Nb doped TiO<sub>2</sub> (red). Black line represents anatase TiO<sub>2</sub> nanocrystalline pattern 98-010-6854.<sup>2</sup>

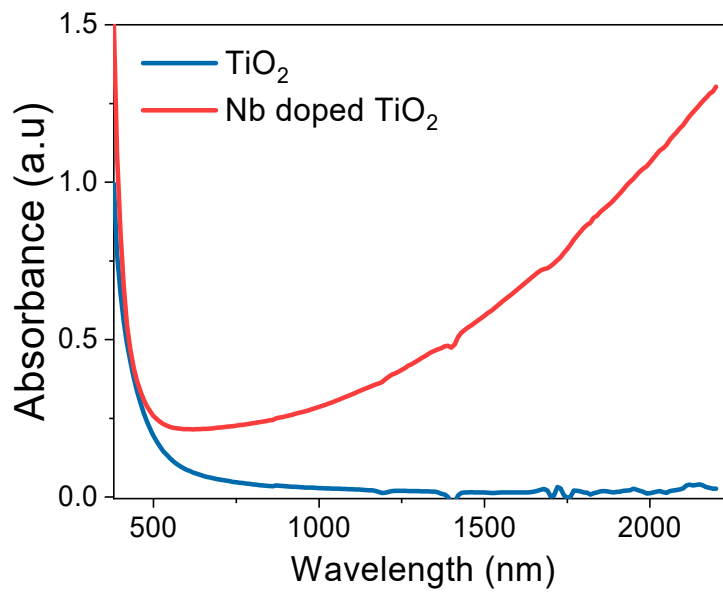


**Figure S3.** UV-vis-NIR absorption curves of bare and Nb doped NCs equimolar in titanium dispersed in hexane.

## S4. Thin film preparation and characterisation

### Thin film cross section

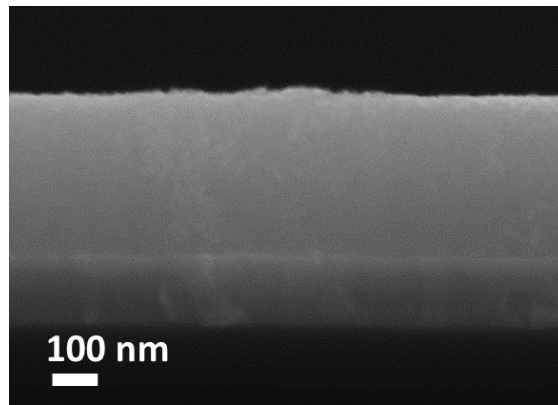


Figure S4. FESEM cross section of Nb doped TiO<sub>2</sub> thin film.

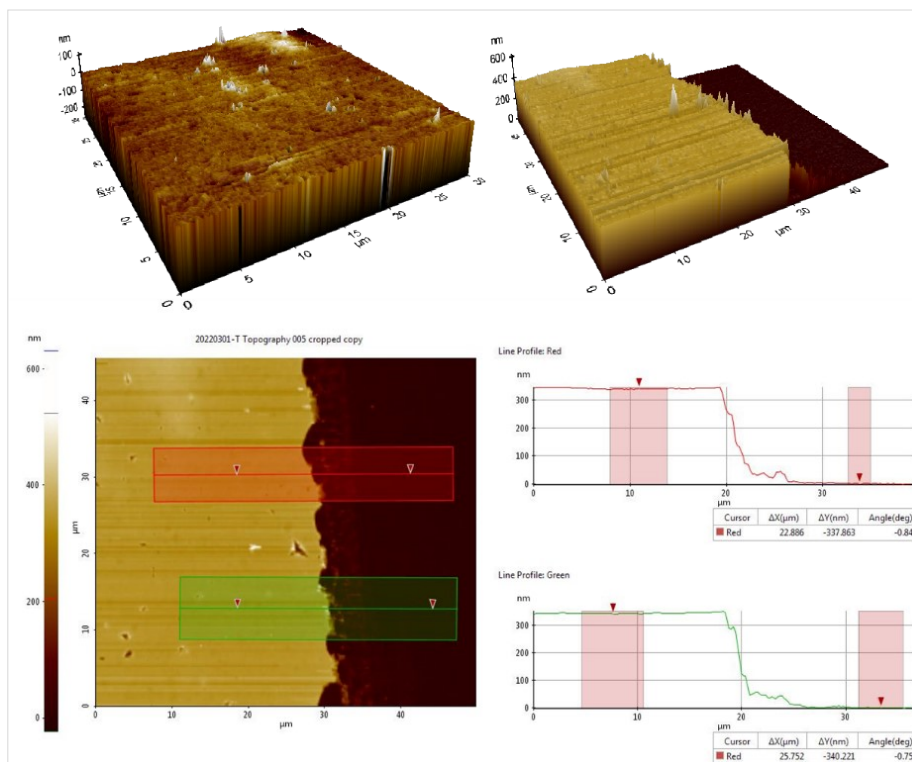


Figure S5. AFM analysis of Nb doped TiO<sub>2</sub> thin film on ITO covered glass.

EDX analysis of the NCs thin films

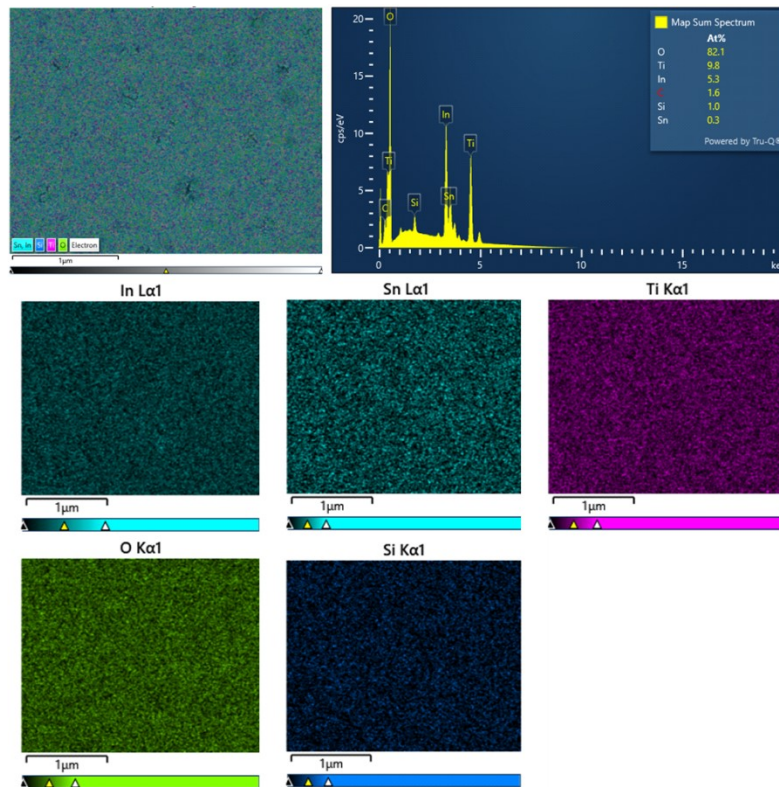


Figure S6. EDX microanalysis of  $\text{TiO}_2$  thin film on ITO covered glass.

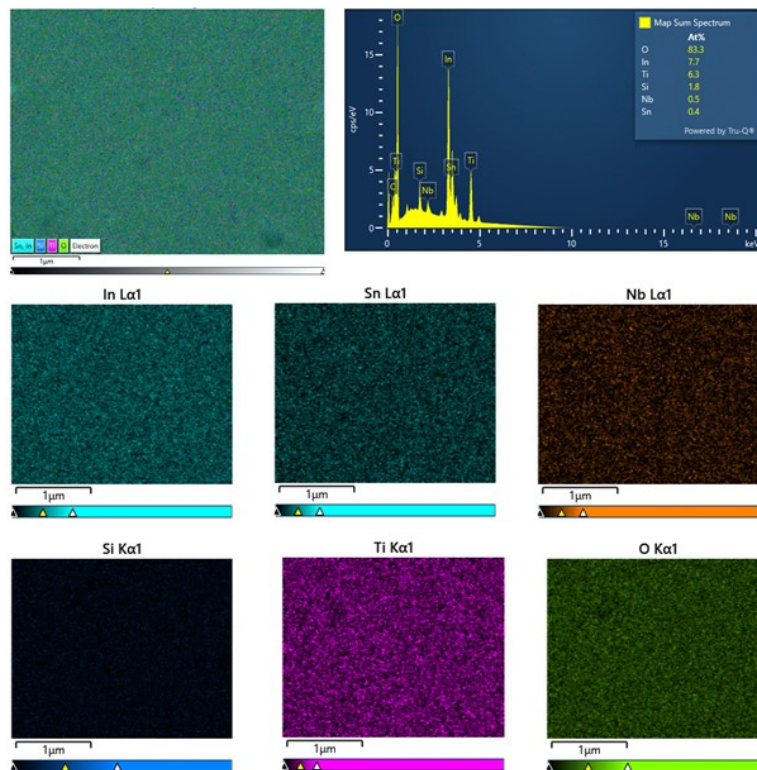


Figure S7. EDX microanalysis of Nb doped  $\text{TiO}_2$  thin film on ITO covered glass.

### S5. Ex situ XANES Ti K Edge

To analyse in depth the crystalline structure of the NCs and the doping nature, an *ex-situ* XAS investigation of the synthesized systems was carried out. Figure S8 shows the XANES spectra at Ti K-edge of bare where and the spectrum of metallic Ti metal is also shown for comparison. The spectral features of both bare and Nb doped TiO<sub>2</sub> (figure 2) clearly indicate the presence of anatase TiO<sub>2</sub>,<sup>3,4</sup> in agreement with Raman and XRD results.

Clear pre-peak resonances are observed in the energy range 4970-4976 eV and can be associated to a combination of 1s-3d quadrupole transitions (E2) and 1s-p electric dipole transitions (E1). A detail of these resonances is shown in the inset of Figure 2a and 2c insets. Three different contributions A1-A3 can be detected and a precise description of these transitions is found elsewhere.<sup>5,6</sup> For the electric dipole transitions there are two possible interactions: i) hybridization of the empty 4p states of the absorbing atom with the empty 3d states of the nearest metal neighbors *via* the p empty states of the ligand; 2ii) hybridization of the empty 4p and 3d states of the absorbing atom. The contribution of E2 transitions is generally much lower than E1 transitions, however E2 transitions are independent on the neighbor atoms and only depends on the transition within 1s-3d states of the absorbing atom.

On the other side, the influence of neighbor atoms is mainly reflected in the A<sub>2</sub> and A<sub>3</sub> features. The variations of intensity and shape of these two features are extremely clear when doping the structure with Nb<sup>5+</sup> ions and a quite higher absorption of A<sub>2</sub> around 4971 eV is observed. The rising edge, feature B, increases in intensity and the absorption at 0.5 in the normalized scale is slighted shifted towards lower energy for Nb-doped TiO<sub>2</sub>. This could be explained with a partial reduction of Ti<sup>4+</sup> ions to accommodate Nb<sup>5+</sup> species in the structure. Other XANES resonances, features from C to G, do not show relevant changes when adding Nb<sup>5+</sup>, but a shift towards lower energy by 0.4 eV is observed for the G resonance. Similar spectral changes have also been discussed by other authors and assigned to a doping of anatase TiO<sub>2</sub> structure by Nb ions.<sup>7,8</sup>

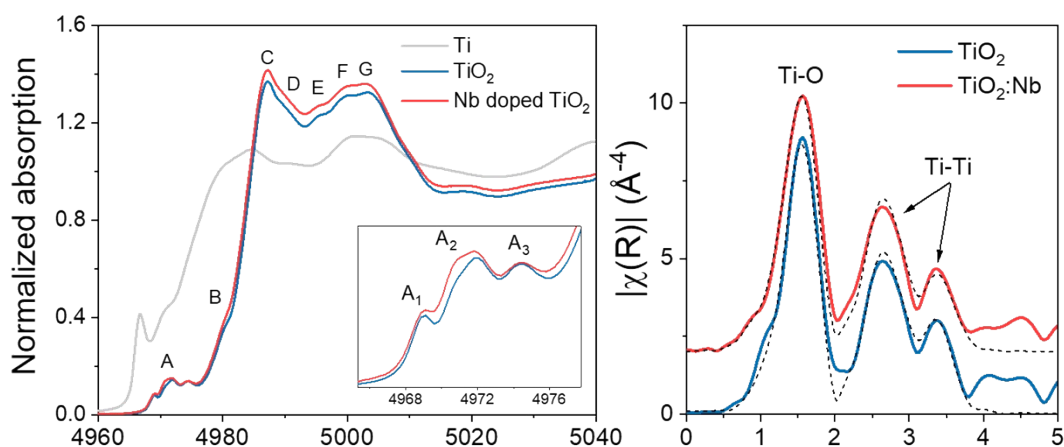


**Figure S8.** a) XANES spectra at Ti K-edge. b) Fourier Transform moduli (solid line) and fit (dashed line) of EXAFS spectra at Ti K-edge for bare and Nb-doped TiO<sub>2</sub> thin films and a Ti metal foil.

**Table S1:** Result of EXAFS fit at Ti K-edge. N is the coordination number, R the bond distance,  $\sigma^2$  the Debye-Waller parameters and  $\Delta E_0$  the energy correction to the inner potential.  $S_0^2$  parameter was obtained by TiO<sub>2</sub> standard and fixed to 0.80.

Sample	Shell	N	R (Å)	$\sigma^2$ (10 <sup>-3</sup> Å <sup>2</sup> )	$\Delta E_0$ (eV)
TiO <sub>2</sub>	Ti-O	6	1.954(4)	5.2(5)	2.0(1.1)
	Ti-Ti	4	3.058(6)	5.2(7)	
	Ti-Ti	4	3.93(5)	13(5)	
TiO <sub>2</sub> :Nb	Ti-O	8	3.80(3)	4(2)	
	Ti-O	6	1.958(4)	7.4(9)	
	Ti-Ti	4	3.054(5)	6.2(6)	
	Ti-Ti	4	3.93(6)	17(6)	
	Ti-O	8	3.83(3)	6(3)	

### S6. Ex situ XANES Nb K edge and DFT calculations

There are clear differences between the spectra (figure 2 in main text) evidencing that Nb<sup>5+</sup> ions are not segregated as Nb<sub>2</sub>O<sub>5</sub> in the TiO<sub>2</sub> structure. In contrast, Nb<sub>2</sub>O<sub>5</sub> has several polymorphs<sup>9</sup> and the reduced intensity of the EXFAS signal can be associated or to destructive interference between several paths and/or to a quite disordered structure

#### Simulation

The simulation was performed considering a substitutional doping in the TiO<sub>2</sub> anatase structure and the crystallographic parameters of the anatase phase were taken from previous XRD results [14]. The as simulated spectrum was shifted in energy to match the measured spectrum and then normalized with the ATHENA software.

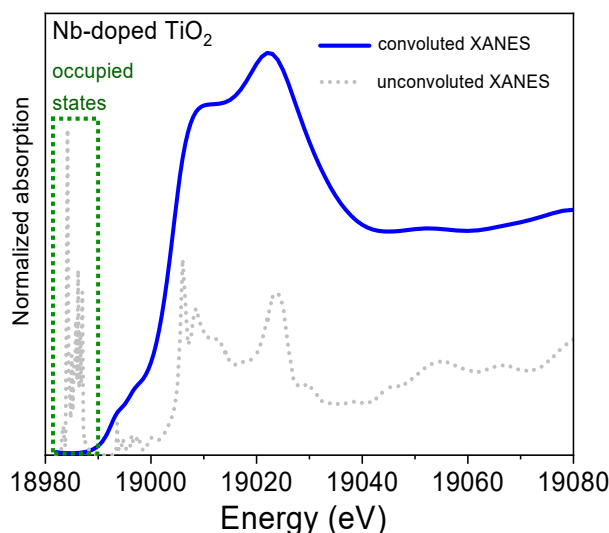


**Figure S9.** Nb K-edge XANES simulation of Nb-doped TiO<sub>2</sub> crystal obtained using FDMNES software. The unconvoluted XANES spectrum was decreased in intensity for a better visualization of the convoluted spectrum.

**Table S2.** Result of EXAFS fit at Nb K-edge. N is the coordination number, R the bond distance,  $\sigma^2$  the Debye-Waller parameters and  $\Delta E_0$  the energy correction to the inner potential.  $S_0^2$  parameter was obtained by Nb foil and fixed to 0.75.

Sample	Shell	N	R (Å)	$\sigma^2$ ( $10^{-3}$ Å <sup>2</sup> )	$\Delta E_0$ (eV)
Nb <sub>2</sub> O <sub>5</sub>	Nb-O	5	2.06(2)	17(1)	7(3)
TiO <sub>2</sub> :Nb	Nb-O	6	2.00(2)	7.8(1.8)	

**Table S3.** Lattice parameters of bare and Nb doped anatase TiO<sub>2</sub> calculated by DFT:

	a	b	c
TiO <sub>2</sub>	11,35316	11,35316	19,18457
Nb-TiO <sub>2</sub>	11,69939	11,69936	19,48059

**Table S4.** Mean distances of the near neighbours Ti-O, Nb-O, Ti-Ti and Ti-O-Ti for bare TiO<sub>2</sub> and Nb-TiO<sub>2</sub>.

	Ti-O Bond (Å)		Nb-O Bond (Å)		Ti-Ti (Å)	Ti-Nb (Å)	Ti-O-Ti (Å)	Ti-O-Nb (Å)
	Equatorial	Apical	Equatorial	Apical				
TiO <sub>2</sub>	1.933	2.001	-	-	3.055	-	3.784	-
Nb-TiO <sub>2</sub>	1.992	2.047	1.954	2.040	3.114	3.166	3.899	3.910

### S7. Electrochemical properties of bare and Nb doped TiO<sub>2</sub>

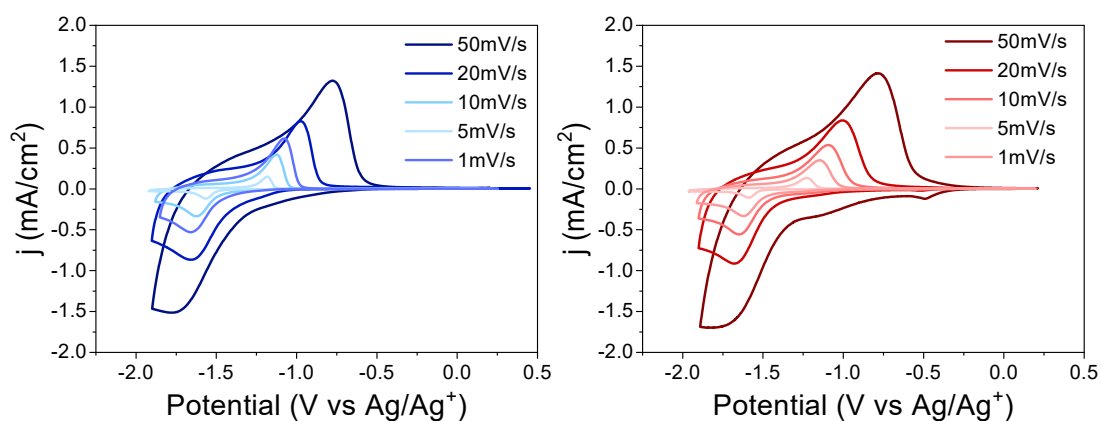


**Figure S10.** CV at different scan rates of bare TiO<sub>2</sub> and Nb doped TiO<sub>2</sub> in 1M LiClO<sub>4</sub> in propylene carbonate.

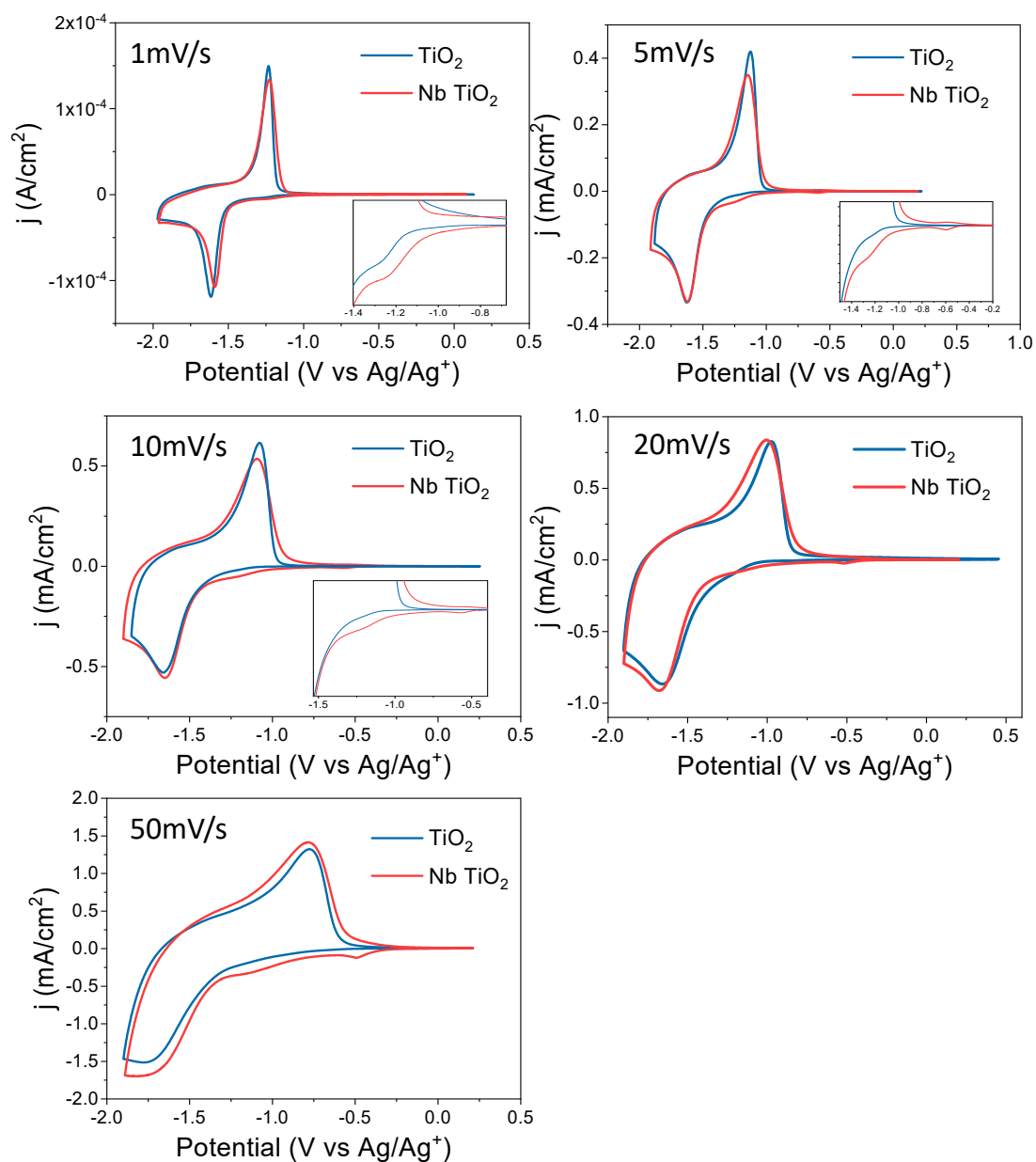


**Figure S11.** Comparison of bare  $\text{TiO}_2$  and Nb doped  $\text{TiO}_2$  Cyclic voltammety's at different scan rates.

## S8. In situ XANES and EXAFS

Average oxidation state after reduction of Ti ions:

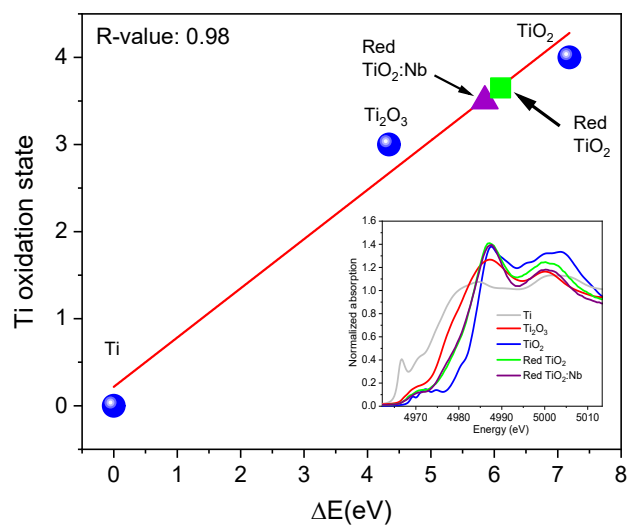


**Figure S12.** Linear dependency of oxidation state on energy shift of references and samples measured at Ti K-edge. The inset shows the XANES spectra of the three references used for the linear fit (Ti,  $Ti_2O_3$  and  $TiO_2$ ) together with the spectra of undoped and Nb-doped  $TiO_2$ .

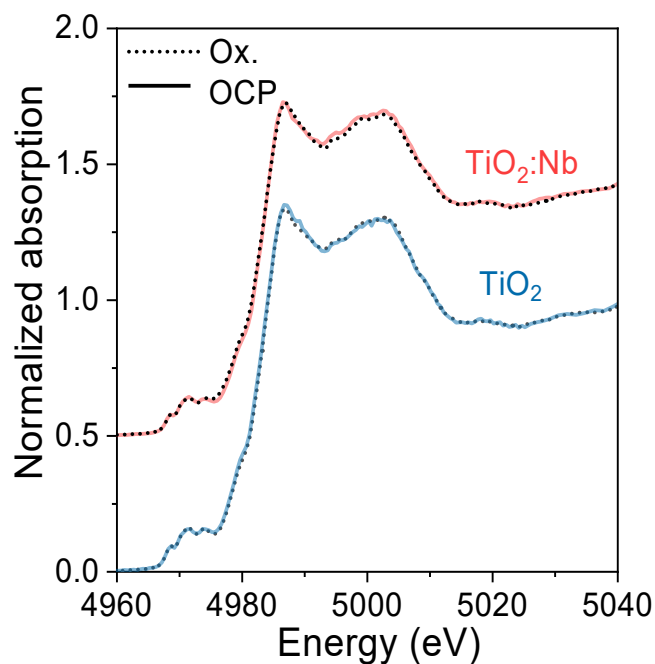


**Figure S13.** XANES Spectra at OCP and oxidised conditions of bare and Nb doped  $TiO_2$ .

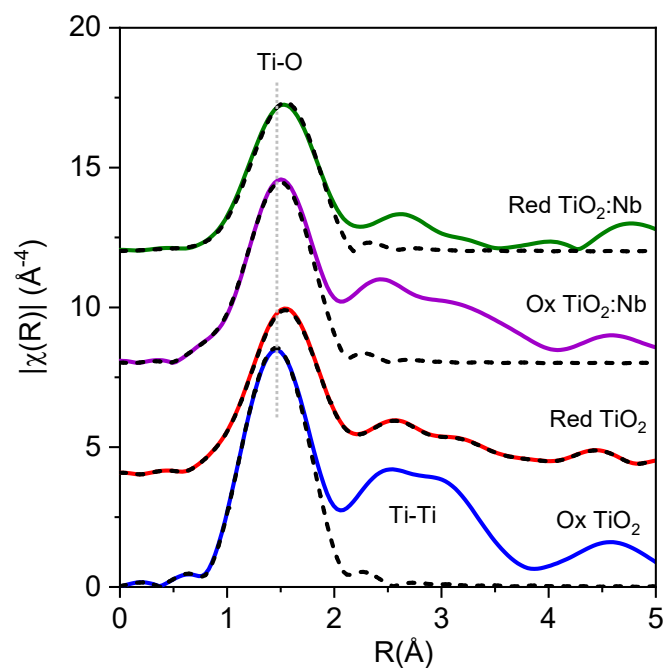


**Figure S14.** Fourier Transform moduli (solid line) and fit (dashed line) of EXAFS spectra at Ti K-edge for undoped and Nb-doped TiO<sub>2</sub> thin films at oxidation and reduction potential. The dashed grey line is a guide for the eye.

**Table S5.** Result of EXAFS fit at Ti K-edge. N is the coordination number, R the bond distance,  $\sigma^2$  the Debye-Waller parameters and  $\Delta E_0$  the energy correction to the inner potential.  $S_0^2$  parameter was obtained by TiO<sub>2</sub> standard and fixed to 0.80:

Sample	Shell	N	R (Å)	$\sigma^2$ ( $10^{-3}$ Å <sup>2</sup> )	$\Delta E_0$ (eV)
Red TiO <sub>2</sub>	Ti-O	6	1.98(1)	7(1)	-2.0(1.2)
Ox TiO <sub>2</sub>	Ti-O	6	1.956(6)	5(1)	
Red TiO <sub>2</sub> :Nb	Ti-O	6	2.01(1)	9.5(9)	
Ox TiO <sub>2</sub> :Nb	Ti-O	6	1.97(1)	7(1)	

### S9. In situ Nb K Edge

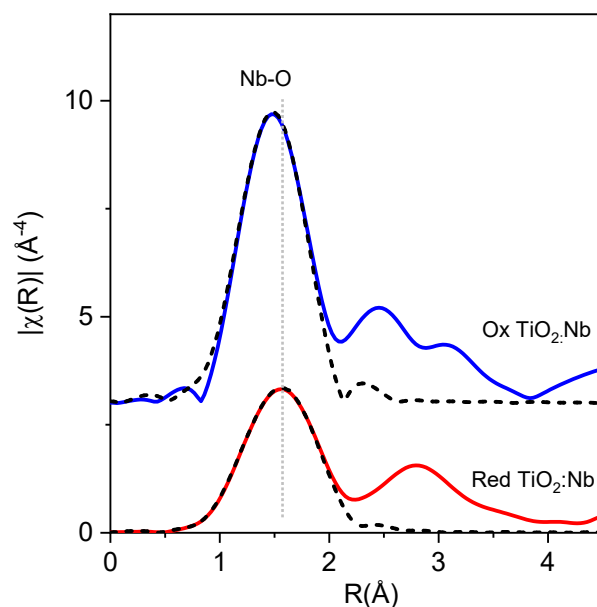


**Figure S15.** Fourier Transform moduli (solid line) and fit (dashed line) of EXAFS spectra at Nb K-edge for undoped and Nb-doped  $\text{TiO}_2$  thin films at oxidation and reduction potential. The dashed grey line is a guide for the eye.

**Table S6.** Result of EXAFS fit at Nb K-edge. N is the coordination number, R the bond distance,  $\sigma^2$  the Debye-Waller parameters and  $\Delta E_0$  the energy correction to the inner potential.  $S_0^2$  parameter was obtained by  $\text{TiO}_2$  standard and fixed to 0.75.

Sample	Shell	N	R (Å)	$\sigma^2$ ( $10^{-3} \text{Å}^2$ )	$\Delta E_0$ (eV)
Red $\text{TiO}_2$	Nb-O	6	1.99(2)	7.2(1.5)	5(3)
Ox $\text{TiO}_2$	Nb-O	6	2.08(2)	13(2)	

### S10. Electrochemical Impedance Spectroscopy

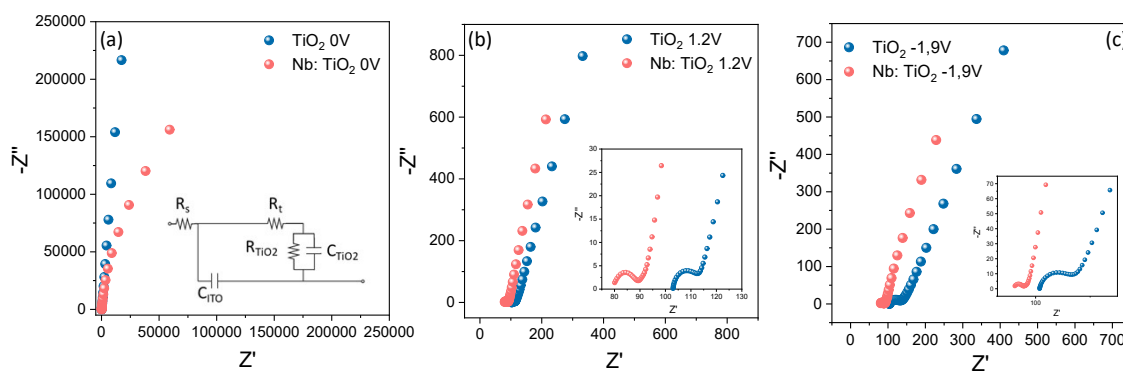


**Figure S16.** Nyquist plots obtained at a) 0, b) -1.2 and c) -1.9 V vs  $\text{Ag}/\text{Ag}^+$  in the analyses samples.

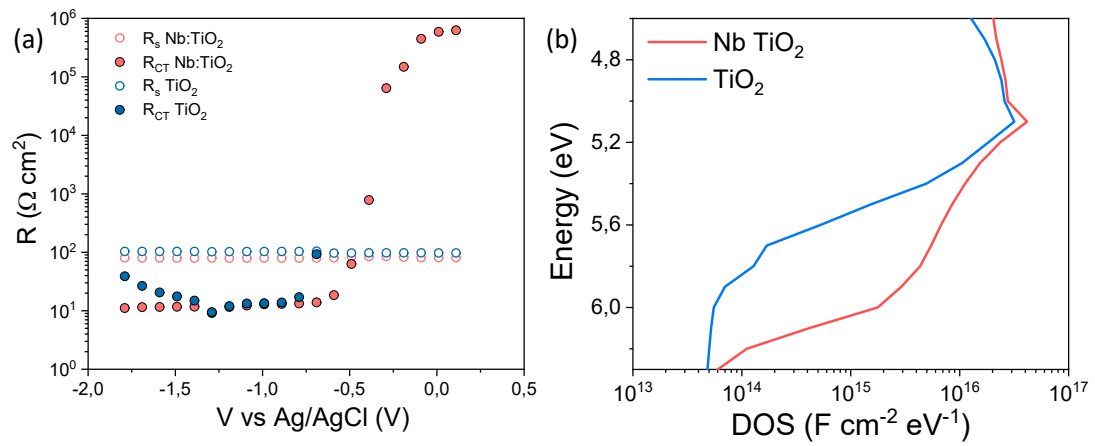


**Figure S17.** a) Extracted resistances and b) density of states from the analyzed samples. The density of states was calculated through the expression:  $C = e \cdot DOS$ , being  $e$  the elementary charge of the electron.

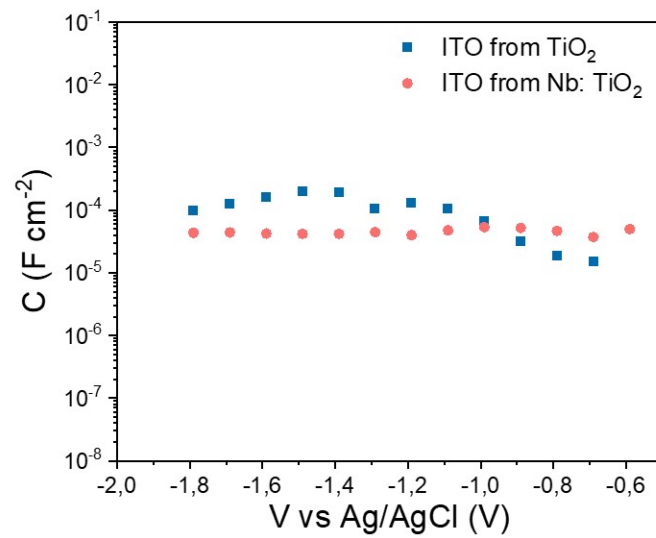


**Figure S18.** Extracted capacitance of ITO substrate from the EIS analysis.

## S11. Smart window device



Figure S19. Images of the smart window lab scale device with high optical transparency.

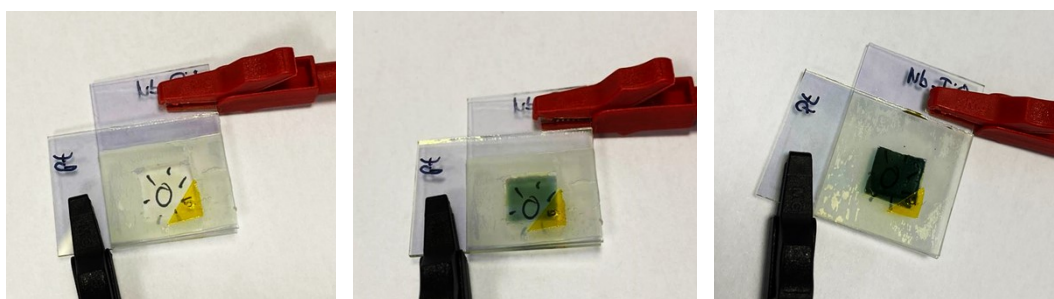


Figure S.20. Smart window device at a) OCP, b) -2.5 and c) -3.5V.

## References

- 1L. De Trizio, R. Buonsanti, A. M. Schimpf, A. Llordes, D. R. Gamelin, R. Simonutti and D. J. Milliron, *Chem. Mater.*, 2013, **25**, 3383–3390.
- 2I. Djerdj and A. M. Tonejc, *Journal of Alloys and Compounds*, 2006, **413**, 159–174.
- 3P. C. Angelomé, L. Andrini, M. E. Calvo, F. G. Requejo, S. A. Bilmes and G. J. A. A. Soler-Illia, *J. Phys. Chem. C*, 2007, **111**, 10886–10893.
- 4F. Fresno, D. Tudela, J. M. Coronado, M. Fernández-García, A. B. Hungría and J. Soria, *Phys. Chem. Chem. Phys.*, 2006, **8**, 2421–2430.
- 5D. Cabaret, A. Bordage, A. Juhin, M. Arfaoui and E. Gaudry, *Phys. Chem. Chem. Phys.*, 2010, **12**, 5619–5633.
- 6F. de Groot, G. Vankó and P. Glatzel, *J. Phys.: Condens. Matter*, 2009, **21**, 104207.
- 7M. Fehse, S. Cavaliere, P. E. Lippens, I. Savych, A. Iadecola, L. Monconduit, D. J. Jones, J. Rozière, F. Fischer, C. Tessier and L. Stievano, *J. Phys. Chem. C*, 2013, **117**, 13827–13835.

- 8 D. S. Bhachu, S. Sathasivam, G. Sankar, D. O. Scanlon, G. Cibin, C. J. Carmalt, I. P. Parkin, G. W. Watson, S. M. Bawaked, A. Y. Obaid, S. Al-Thabaiti and S. N. Basahel, *Adv. Funct. Mater.*, 2014, **24**, 5075–5085.
- 9 H. T. Kreissl, M. M. J. Li, Y.-K. Peng, K. Nakagawa, T. J. N. Hooper, J. V. Hanna, A. Shepherd, T.-S. Wu, Y.-L. Soo and S. C. E. Tsang, *J. Am. Chem. Soc.*, 2017, **139**, 12670–12680.